JOURNAL OF GEOPHYSICAL RESEARCH, VOL. 103, NO. C5, PAGES 10,223–10,239 MAY 15, 1998

Spreading of Labrador Sea Water in the eastern North Atlantic

Jérôme Paillet
Service Hydrographique et Oceanographique de la Marine, Brest, France

Michel Arhan
Laboratoire de Physique des Oceans, IFREMER, Centre de Brest, Plouzané, France

Michael S. McCartney
Woods Hole Oceanographic Institution, Woods Hole, Massachusetts

Abstract. The spreading of Labrador Sea Water (LSW) in the eastern North Atlantic south of 55°N is described on the basis of recent, high-resolution hydrographic lines and using an inverse model of that basin general circulation. The isopycnic "salinity anomaly" relative to a standard θ/S curve is used to detect the main branches and limits of dominant influence of the intermediate water masses. The LSW crosses the Mid-Atlantic Ridge at latitudes around 50°N with parts spreading farther eastward and southward. One southward pathway along the eastern side of the Mid-Atlantic-Ridge stands out as an eastern basin counterpart of the western Atlantic "Deep Western Boundary Current." An entry into the Bay of Biscay in its northern part is also evidenced with striking similitudes between two data sets from 1974 and 1989–1990. At the southern limit of the LSW extension, in the vicinity of the Azores-Biscay Rise, a marked front exists basinwide around 1800 m with the more saline Deep Mediterranean Water (DMW). The inverse model velocity field is consistent with most features of the tracer distributions and allows estimation of LSW transports: 6.3 ± 1.2 Sv of LSW with salinities lower than 34.94 cross the 35°W meridian eastward between 44°N and 54°N, one fourth of which recirculates southwestward in the western basin, while another fourth turns northward across 54°N and the remaining half proceeds southward in the eastern basin. The model circulation suggests that DMW results from mixing between eastern basin LSW and the overlying Mediterranean Outflow Water, most probably through double diffusion. We finally describe several mesoscale structures of anomalously high LSW influence south of the LSW-DMW front, notably one sampled by a RAFOS float. The velocity and potential vorticity fields suggest that these "LSW-eddies" are formed through baroclinic instability at the LSW-DMW front.

1. Introduction

The presence of water originating from the Labrador Sea at intermediate depths in the eastern North Atlantic has often been reported and analyzed, notably by *Pingree* [1973], *Talley and McCartney* [1982], *McCartney* [1992], and *Cunningham and Haine* [1995a]. They used the vertical anomalies of salinity, potential vorticity, or dissolved oxygen associated with the "Labrador Sea Water" (LSW) to map its distribution and to infer its circulation, particularly its eastward crossing of the Mid-Atlantic Ridge (MAR) around 52°N, above the Charlie Gibbs Fracture Zone. *Talley and McCartney* [1982] and *Harvey and Arhan* [1988] observed that the signals associated with the LSW in the depth range 1500–2500 m extend south of that latitude in the eastern basin, this extension being limited by a boundary with more saline water around 40°N. The latter, called Deep Mediterranean Water (DMW) by *Harvey and Arhan* [1988], should be distinguished from the "Mediterranean Outflow Water" (MOW) issued from the Straits of Gibraltar that stabilizes in the North Atlantic in the depth range 700–1500 m. The DMW acquires its relatively high salinity through vertical mixing with the overlying MOW. *Tsuchiya et al.* [1992] and *Arhan et al.* [1994], analyzing individual high-resolution hydrographic lines, showed that this LSW-DMW boundary is a sharp thermohaline front with only a weak density signature.

Our present knowledge of the LSW distribution in the eastern North Atlantic rests on the aforementioned analyses of basinwide but rather low-resolution data sets and of individual high-resolution sections. The description of its circulation in that basin has been so far mostly inferred from tracers distributions. More quantitative estimations of velocities or transports were made difficult by the sparseness of direct measurements and by the depth range considered being close to generally assumed levels of no motion. Some of the few quantified results are those of *Saunders* [1982], who computed averaged meridional geostrophic velocities referenced to 4000 m over the width of the eastern basin. Net equatorward transports between about 3×10^6 m^3 s^{-1} (at 48°N) and 10^6 m^3 s^{-1} (at 32°N) in the depth range 1500–2500 m are deduced from that study, which confirms the tracer-inferred southward spreading but gives no details of the two-dimensional circulation. More details were proposed in several papers showing inverse model results, notably the North Atlantic model of *Bogden et al.* [1993] based on the *Levitus* [1982] climatology,

Paper number 98JC00262.
0148-0227/98/98JC-00262$09.00

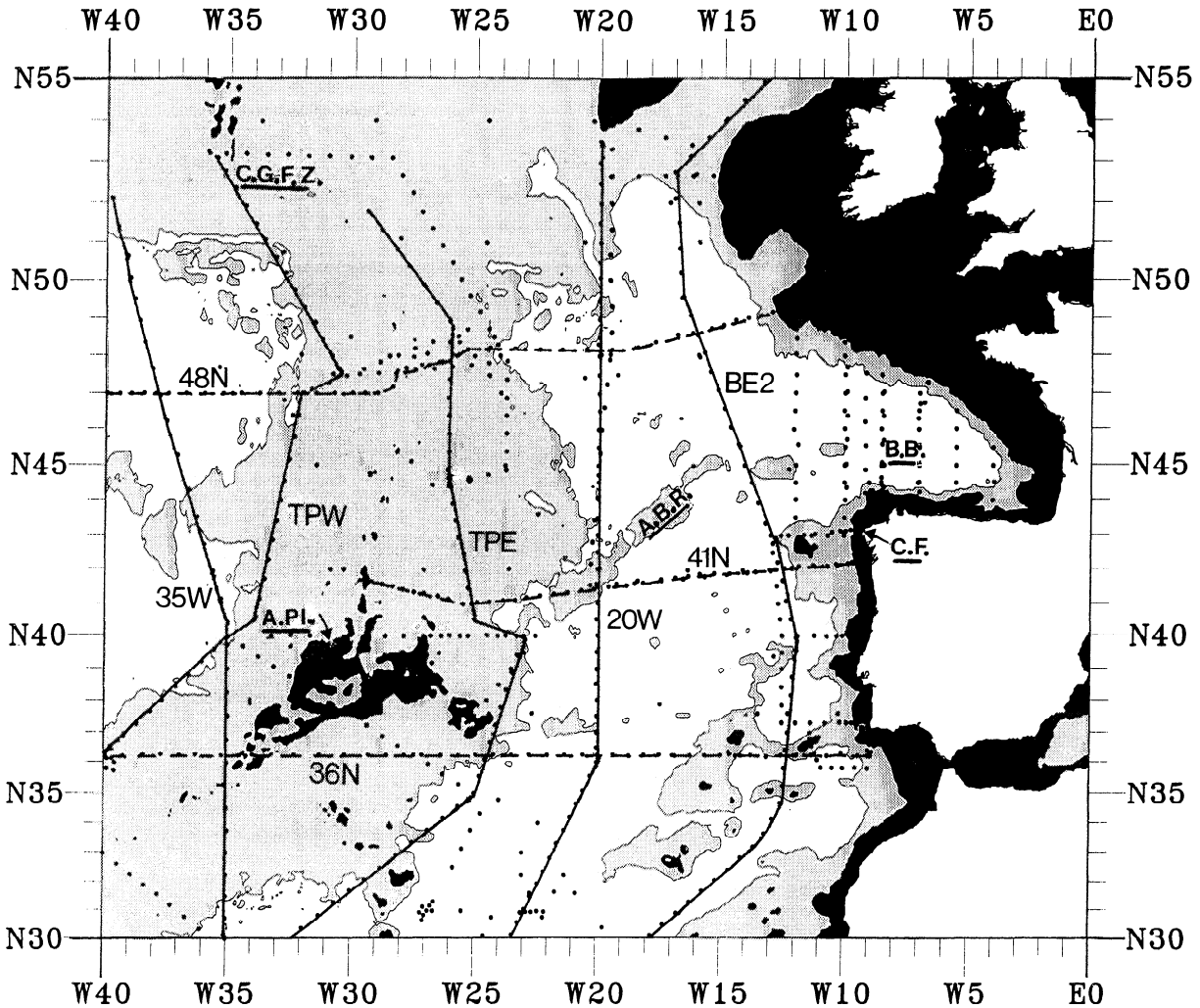

Figure 1. CTD data set. The solid lines mark the transects used in sections 2 and 3. Solid (shaded) areas show where the bottom depth is shallower than 1800 m (between 1800 and 4000 m). Underlined abbreviations stand for CGFZ, Charlie Gibbs Fracture Zone; APl, Azores Plateau; ABR, Azores-Biscay Rise; BB, Bay of Biscay; CF, Cape Finisterre.

that of *Gana and Provost* [1993], based on the TOPOGULF data set of 1983–1984, and that of *Paillet and Mercier* [1997] of the eastern North Atlantic, based on recent (1981–1993) hydrographic data. These studies provide views of the velocity fields at 2000, 2750, and 2500 m, respectively, and confirm the southward flow of LSW in the eastern basin, yet without fully quantifying it. Furthermore, these inverse models using gridded and smoothed hydrographic data cannot show the details of the small-scale currents, veins, or branchings.

Recent studies have also focused on LSW to evidence climate change or decadal variability signals. *Lazier* [1981] and *Talley and McCartney* [1982], studying the hydrography of the central Labrador Sea, first showed that there is a large interannual variability in the strength of wintertime convection which induces a variability in the properties of the newly formed LSW. *Cunningham and Haine* [1995a, b] showed that as a consequence of these source variations, the LSW in the eastern North Atlantic was not in a steady state in 1991. *Curry et al.* [1998] revisited the whole North Atlantic hydrographic data set since 1950 to link subtropical signals in the deep layers with the variability of the convection regime in the subpolar latitudes. Despite these changes in the LSW properties, its large-scale circulation was shown to present relatively steady patterns over the different sampling periods.

The first goal of this paper is to take advantage of numerous high-resolution CTD transects (Figure 1 and Table 1) carried out in the eastern North Atlantic from the mid-1970s to the late 1980s to infer the distributions and limits of influence of the LSW and the DMW during that period. For that purpose, in section 2 we define a "salinity anomaly" relative to a standard θ/S curve. That conservative tracer vanishes at the LSW-DMW boundary, thus revealing under which dominant water mass influence each fluid particle is. The salinity anomaly is displayed along the high-resolution hydrographic lines in section 3 to provide information on the eastward spreading of LSW above the MAR, its subsequent branching in the eastern basin, and its boundary with the DMW.

The second goal of this paper is to provide direct estimates of the geostrophic transports at the LSW level in the eastern North Atlantic, using a method that is not very sensitive to the choice of a reference level. A slightly modified solution of the inverse model of *Paillet and Mercier* [1997] is analyzed in section 4 to study the LSW circulation and to discuss the question of the DMW origin.

Table 1. Data Description and Abbreviations Used in the Text and in Figures 1 and 7

Cruise	Abbreviation	Dates	Institution	Data Description	Ship
PHYGAS 42	···	June–July 1974	CNEXO	*Fruchaud-Laparra et al.* [1976]	*Cryos*
Discovery 81	41N	Jan. 1977	IOS/Wormley	*Saunders* [1982]	*Discovery*
Atlantis 109	36N	June–July 1981	WHOI	*Roemmich and Wunsch* [1985]	*Atlantis II*
TTO-NAS	···	July 1981	SIO and WHOI	*SIO* [1986]	*Knorr*
Hudson 82	48N	April 1982	BIO	*Hendry* [1989]	*Hudson*
Knorr 104	35W	July–Aug. 1983	WHOI	*McCartney* [1992]	*Knorr*
Topogulf	TPW, TPE, 40N, and SAZ	Aug.–Sept. 1983 Aug. 1984	IFREMER Brest and IFM Kiel	*Topogulf Group* [1986]	*Le Suroit Poseidon Meteor*
Bord-Est 2	BE2	May–June 1988	IFREMER Brest	*Arhan et al.* [1991a]	*Jean Charcot*
Oceanus 202	20W	July–Aug. 1988	WHOI	*Tsuchiya et al.* [1992]	*Oceanus*
Discovery 181	···	April 1989	IOS/Wormley	*Read et al.* [1991]	*Discovery*
Bord-Est 3	···	May 1989	IFREMER Brest	*Arhan et al.* [1991b]	*Le Noroit*
Discovery 189	···	March 1990	IOS/Wormley	*King et al.* [1991]	*Discovery*
Vivaldi	···	April–June 1991	IOS/Wormley	*Griffiths et al.* [1992]	*Charles Darwin*

CNEXO, Centre National pour l'Exploration des Oceans; IOS, Institute of Oceanographic Sciences; WHOI, Woods Hole Oceanographic Institution; SIO, Scripps Institution of Oceanography; BIO, Bedford Institute of Oceanography; IFREMER, Institut Français de Recherche pour l'Exploitation de la Mer; IFM, Institut für Meereskunde.

Finally, this study provides evidence of high mesoscale activity near the thermohaline front separating LSW and DMW, a likely result of instability of that front. We analyze in section 5 the presence of mesoscale structures in the high-resolution hydrographic sections and the behavior of a Lagrangian float that was launched in such an eddy during the Structure des Echanges Mer-Atmosphere, Proprietes des Heterogeneites Oceaniques: Recherche Experimentale (SEMAPHORE) 1993 experiment.

2. A Salinity Anomaly Relative to a Standard θ/S Curve

Over most of its spreading area, the LSW is characterized by a salinity minimum due to the excess of freshwater input over evaporative loss in the Labrador Sea and by the potential vorticity minimum and oxygen maximum due to its formation by deep winter convection. However, the disappearance of such vertical extrema does not necessarily mark the limit of influence of the water mass. Being interested in the thermohaline front between the LSW and the DMW, for this study we chose to use a salinity anomaly ΔS relative to a "standard" θ/S curve representative of the eastern North Atlantic, a quantity vanishing at the front. The sign of ΔS thus shows under which dominant water mass influence any considered particle is. Figure 2 displays the θ/S scatter plots along the three transects 35W, 20W, and BE2 (see Figure 1), together with the standard θ/S curve defined as follows:

At potential temperatures >10°C, it is parallel to the curve proposed by *Armi and Bray* [1982] for the western basin and goes through the point $\theta = 10°C$, $S = 35.35$. It matches the central water θ/S relation of that basin (Figure 2, top).

For $4°C < \theta < 10°C$, the standard curve is linear between the points [10°C, 35.35] and [4°C, 35.0]. In that temperature range it separates the MOW, characterized by positive anomalies, from the Sub-Arctic Intermediate Water (SAIW) characterized by negative anomalies.

For $2.5°C < \theta < 4°C$, the standard curve (Figure 2, bottom) is linear between the points [4°C, 35.0] and [2.5°C, 34.943]. At these temperatures it separates the LSW, characterized by a salinity minimum, from the DMW that presents positive anomalies. The θ/S plots of the 20W and BE2 transects illustrate the frontal character of the boundary between these water masses, most individual profiles being markedly on one side or the other of the standard curve.

For $\theta < 2.5°C$, we use the standard curve defined by *Saunders* [1986] for the deep waters of the eastern North Atlantic:

$$S = 34.698 + 0.098\theta$$

The salinity anomaly ΔS is defined as the isopycnal salinity difference between a θ/S point and the standard curve, that is, the difference in salinity between the point and that on the standard curve having the same potential density (referred to a neighboring pressure level).

It has been known since the work by *Lazier* [1981] that there are year-to-year changes in the properties and rates of formation of LSW in the central Labrador Sea, and we may wonder to what extent these variations affect the LSW ΔS values in the eastern North Atlantic. *Cunningham and Haine* [1995a, b] show that the LSW vintages present in that basin in 1991 were comprised between 1972 and 1986. It can thus be estimated that the LSW seen in our 1974–1991 data set was formed between 1950 and 1986. *Curry et al.* [1998] provide a continuous series of the annual mean θ and S values of the LSW core inside the central Labrador Sea. From 1949 to 1986 the salinity anomaly in that "young" LSW core varied between −0.085 (in 1970) and −0.137 (in 1974). The amplitude of these variations is thus of order 5×10^{-2}. *Cunningham and Haine* [1995b], analyzing the advective-diffusive balance of the LSW, show that the salinity gradients due to variability at the source are typically reduced by a factor of 5 before entering the eastern basin. One may thus expect that the source-induced variations of ΔS do not exceed 10^{-2} in the eastern basin. Below we analyze geographical variations of ΔS that are of the order of 2.5×10^{-2} or more, i.e., well beyond those expected from interannual variability during that period.

3. Spreading of LSW and DMW in the Eastern North Atlantic

3.1. Eastward Spreading of LSW Around 50°N

As the LSW enters the eastern North Atlantic as a mainly zonal intrusion around 50°N [*Talley and McCartney*, 1982], Figure 3 shows the average profiles of ΔS and of the large-scale potential vorticity $q = fN^2/g$ (where f is the Coriolis

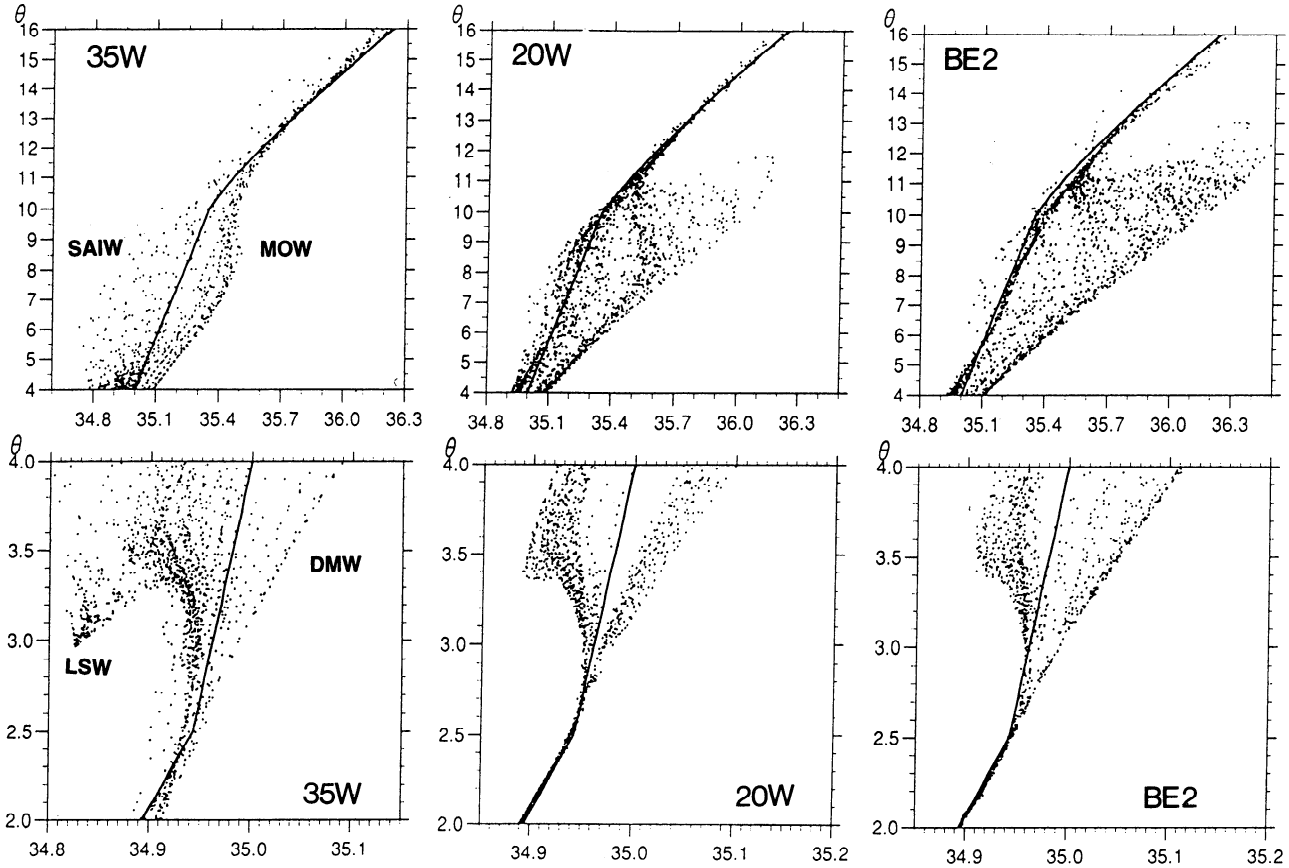

Figure 2. The θ/S plots along the 35W, 20W, and BE2 lines. The solid line is the "standard" θ/S relation used to estimate ΔS. Intermediate water masses are shown on the 35W diagram: SAIW, Subarctic Intermediate Water; MOW, Mediterranean Outflow Water; LSW, Labrador Sea Water; DMW, Deep Mediterranean Water.

parameter, g is the gravity acceleration, and N^2 is the squared Brunt Väisälä frequency) between 48°N and 52°N on the quasi-meridional lines 35W, 20W, and BE2. On each line, LSW stands out as a q minimum (Figure 3b) centered near 1500 m on 35W, 1750 m on 20W, and 1800–2000 m on BE2. It also appears as a ΔS minimum on 20W and BE2 (Figure 3a), below the maximum associated with MOW at around 1000 m depth. On 35W, located to the west of the MAR, LSW is not visible

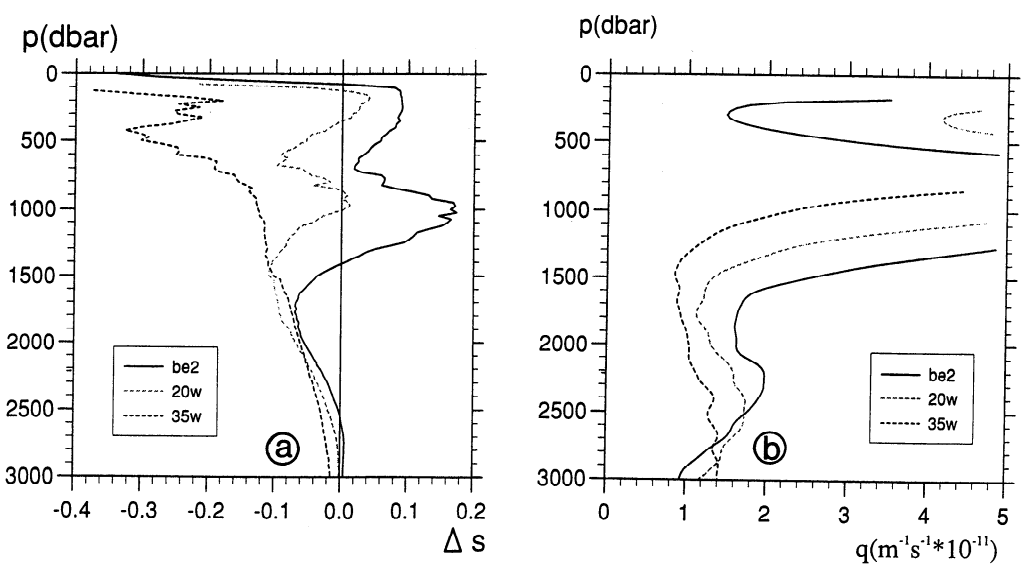

Figure 3. Mean profiles of (a) ΔS and (b) q in the 48°N–52°N latitude range, along the 35W, 20W, and BE2 lines.

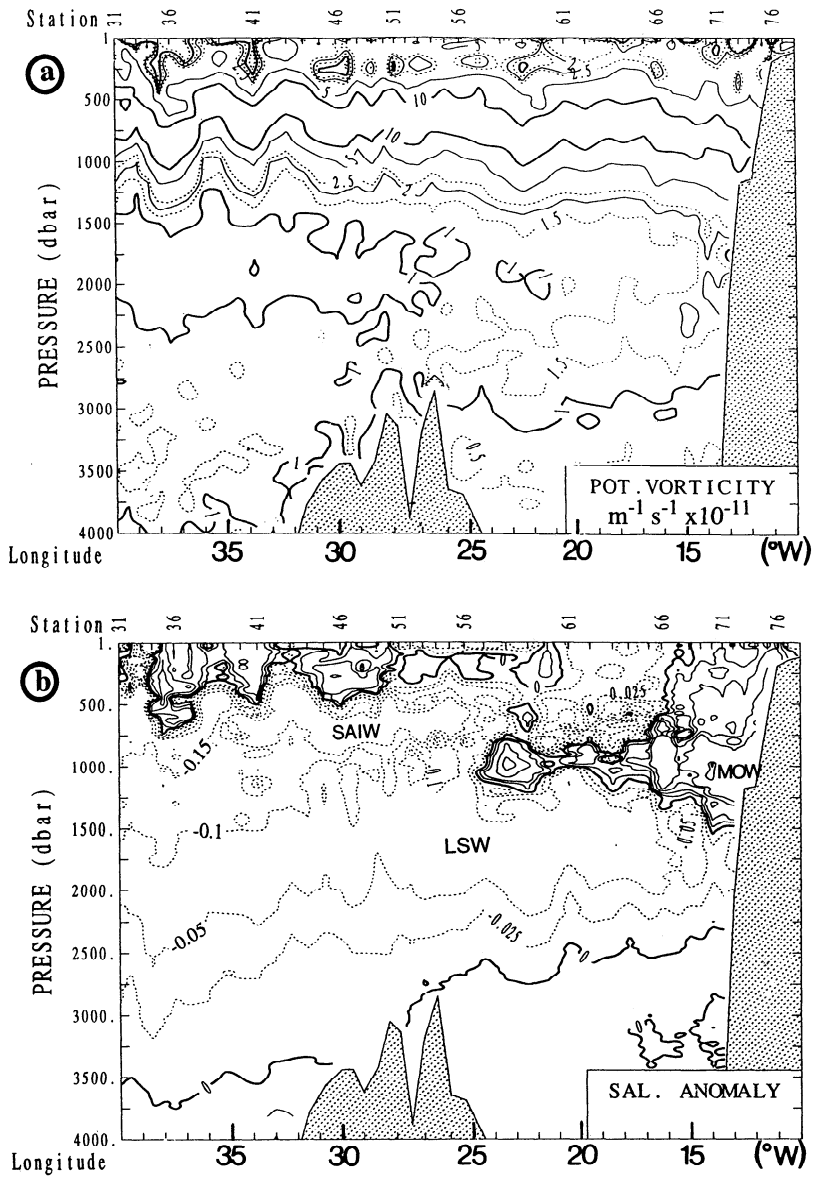

Figure 4. Vertical distributions of (a) q and (b) ΔS along the 48N line. ΔS isocontours are ± 0.15, ± 0.1, ± 0.05, ± 0.025, 0. Abbreviations are SAIW, Subarctic Intermediate Water; MOW, Mediterranean Outflow Water; LSW, Labrador Sea Water.

as a ΔS minimum because the overlying water there is SAIW, which has even lower ΔS values. Figure 3 suggests that while flowing eastward, the LSW between 48°N and 52°N experiences deepening and restratification (q increases eastward), whereas ΔS is approximately conserved between 1700 and 2000 m.

Another illustration of the eastward spreading of LSW in the eastern North Atlantic is provided by the vertical sections of q and ΔS along line 48N, displayed in Figure 4. The potential vorticity section (Figure 4a) shows the continuity across the MAR of the minimum at 1800 dbar associated with the LSW and the eastward increase of the q values along the minimum. The LSW is also seen from its low ΔS values, below 1000 dbar, in Figure 4b. As noted above, these low values constitute a vertical minimum only in the eastern part of the basin where MOW is found. The ΔS values are quite homogeneous in the LSW tongue east of the MAR. Figure 4 provides a striking confirmation of the fact, first mentioned by *Pingree* [1973], that the LSW reaches the North Atlantic eastern boundary. Noting, in Figure 4a, that the water above 1000 dbar (either the fresh SAIW or the saline MOW) has a high potential vorticity ($>5 \times 10^{-11}$ m^{-1} s^{-1}) throughout the basin, we decide in the following to call "LSW" the water with negative ΔS values located deeper than 1000 dbar.

3.2. Meridional Extension of LSW and Thermohaline Front With DMW

Figure 5 shows the vertical distributions of ΔS along seven hydrographic transects (35W, TPW, TPE, 20W, BE2, 41N, and 36N, see Figure 1) that were carried out between 1977 and 1988 (Table 1). In this section we only describe the large-scale water mass distribution, smaller-scale structures being analyzed in section 5.

The two westernmost sections 35W and TPW (Figures 5a

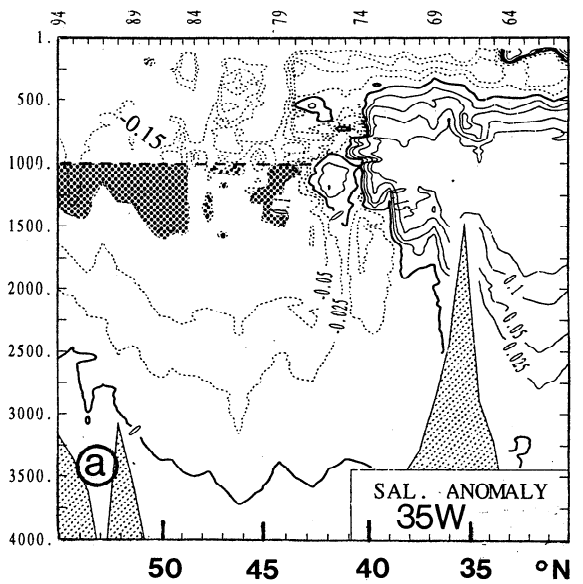

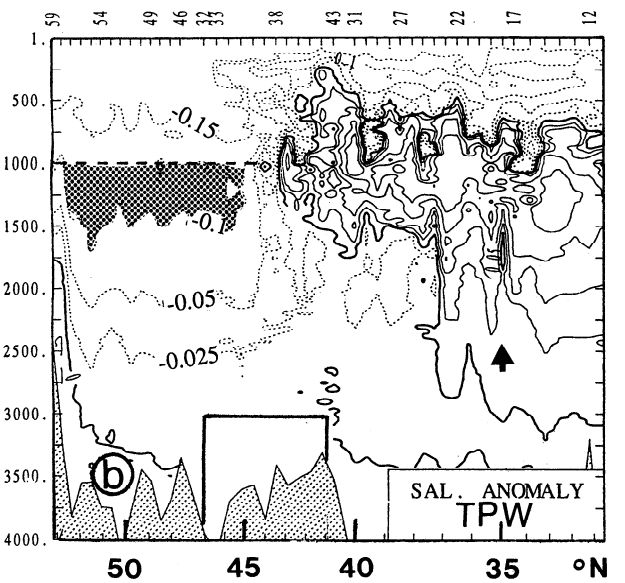

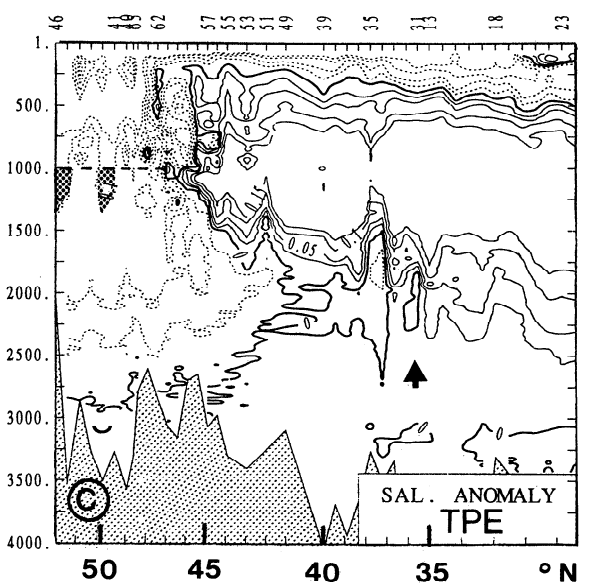

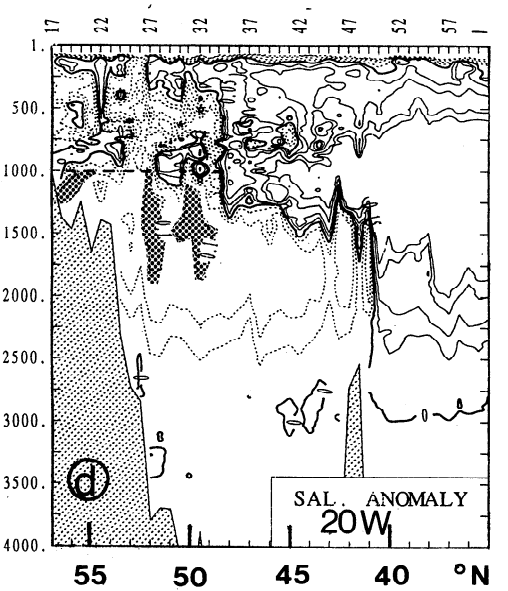

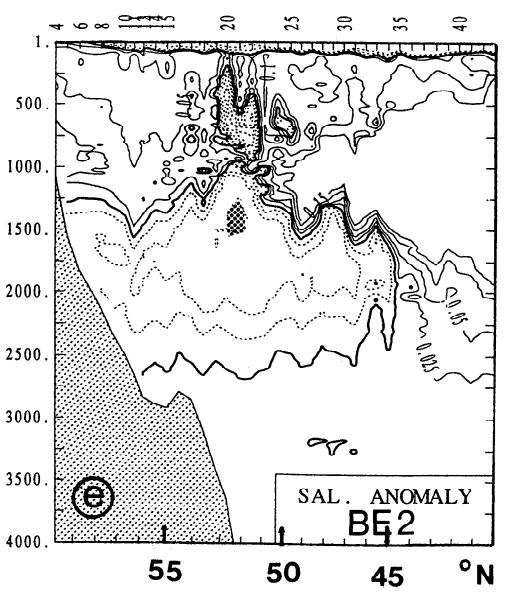

Figure 5. Vertical distributions of ΔS along the quasi-meridional lines (a) 35W, (b) TPW, (c) TPE, (d) 20W, and (e) BE2 and along the quasi-zonal lines (f) 41N and (g) 36N. Shaded areas show the LSW of $\Delta S < -0.1$ (below 1000 dbar). Arrows mark submesoscale LSW structures described in section 6.

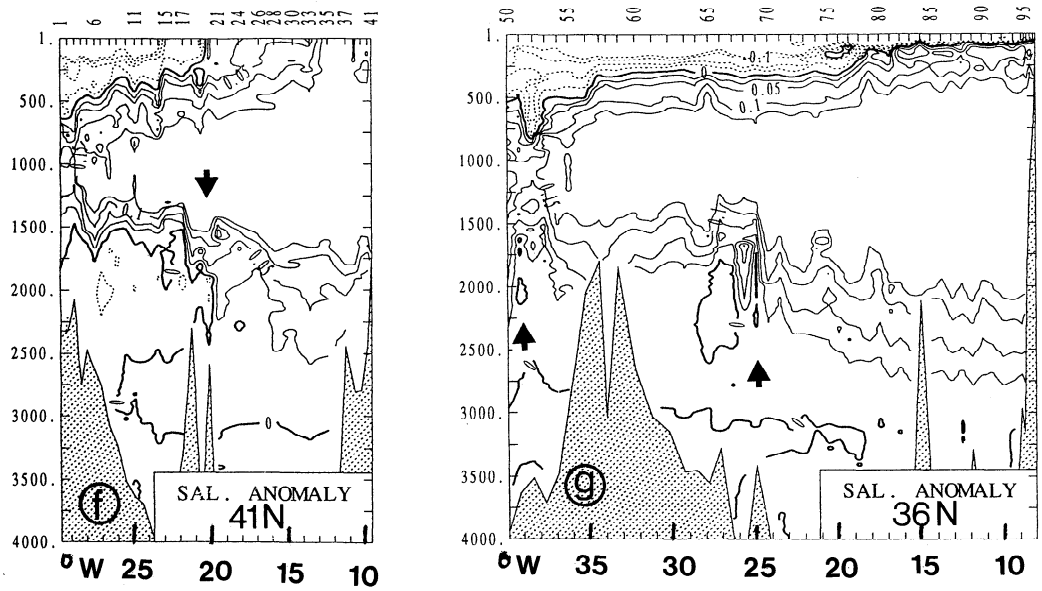

Figure 5. (continued)

and 5b) show the presence of LSW north of about 37°N above the western flank of the MAR. The large domain with $\Delta S < -0.1$, located at 49°N–55°N on 35W and 45°N–52°N on TPW, corresponds to *Talley and McCartney*'s [1982] "eastern branch" which flows toward the eastern basin. On TPW this branch is bounded on its northern side, below 1700 dbar, by a water mass of positive ΔS which is a vein of Iceland–Scotland Overflow Water (ISOW), flowing westward along the northern wall of Charlie Gibbs Fracture Zone. The southward extensions of the negative ΔS domain on both lines suggest that while a part of the LSW carried in this branch proceeds to the eastern basin, another part remains west of the MAR to experience further southward spreading.

In the eastern basin the three quasi-meridional sections TPE, 20W, and BE2 (Figures 5c, 5d, and 5e) complement the illustration provided by 48N (Figure 4) of the eastward progression of the LSW. Two LSW cores with low ΔS values (< -0.1) are detectable on either side of 50°N, along TPE and 20W. Only one core, at 52°N, is still found along BE2 (Figure 5e), suggesting that the other branch has recirculated southward before reaching the BE2 line. In the northern part of BE2, LSW is seen extending northward into the Rockall Trough, where it constitutes the bottom water. At 1800 m the transition between LSW and DMW is very sharp at 41°N along 20W and at 45°N along BE2, as previously noted by *Tsuchiya et al.* [1992] and *Arhan et al.* [1994]. In both cases the boundary is close to the Azores–Biscay Rise, a deep ridge oriented SW-NE (Figure 1). Along TPE, a first LSW-DMW transition appears at about 41°N, coinciding with an eastward shift of the line axis (see Figure 1), but a large patch of LSW influence also exists between 37°N and 40°N. The abrupt boundary with DMW is found at 37°N, near a topographic high to the east of the Azores Islands.

Along the 41N section (Figure 5f), LSW is present only in the western part of the basin, and the transition with DMW at 20°W again coincides with the Azores-Biscay Rise. From sections TPE, 20W, BE2, and 41N in Figure 5 it is therefore clear that most of the LSW found in the eastern North Atlantic is located northwest of that topographic ridge. The 36N section (Figure 5g), however, shows that the LSW penetrates as far south as 36°N near the MAR, slightly negative ΔS values being found between 26°W and 29°W. Further evidence for the existence of a vein of LSW flowing along the eastern side of the MAR is given in section 3.3.

Examination of the ΔS values at the intersections of the lines in the eastern basin shows an overall agreement to within 0.025 between the different lines at the LSW-DMW level, a number that drops to about 0.01 when local mesoscale perturbations are filtered out. The large-scale ΔS field thus seems to have remained quite steady during the sampled period, suggesting that a mapping from the nonsynoptic sections should be representative of the mean for that period. Figure 6 shows the minimum of ΔS in the density range $32.25 < \sigma_{1,2} < 37.00$ at each station of the whole data set. The mapping was done using a four-point bilinear interpolation on a 1° resolution grid that is aimed at smoothing the data as little as possible. In the eastern basin, LSW is seen by its $\Delta S < 0$ values to the northwest of a line joining [35°N, 25°W] to [47°N, 8°W], close to the limit quoted by *Talley and McCartney* [1982] from their 1955–1964 data set, south of which LSW also becomes undetectable by its potential vorticity minimum. It is parallel to, and slightly south of, the main axis of the Azores-Biscay Rise (Figure 1).

Having noted that the source variations of ΔS should be smaller than 10^{-2} and the ΔS parameter being conserved except for mixing effects, the circulation is expected to be mostly "along tongues" of equal ΔS. The isopleths of Figure 6 then reveal that the main branch of LSW flows into the eastern basin above the MAR, seen as a tongue of $\Delta S < -0.125$ centered around 51°N–52°N, its broad southward recirculation in the latitude range 42°N–50°N in the middle of the eastern basin, suggested by the bulging of isopleths -0.025 to -0.1, and its further southwestward flow toward the vicinity of the Azores Plateau, evidenced by the zero contour. A close look at isopleths -0.025 and 0.0 also suggests a clockwise flow around the Azores Plateau and an entry into the northern half of the Bay of Biscay, these points being discussed in more detail in sections 3.3 and 3.4. Although some spatial smoothing ensues from taking the minimum of ΔS in a wide density range and from the mapping technique itself, a few mesoscale structures that should not be regarded as permanent are visible as small

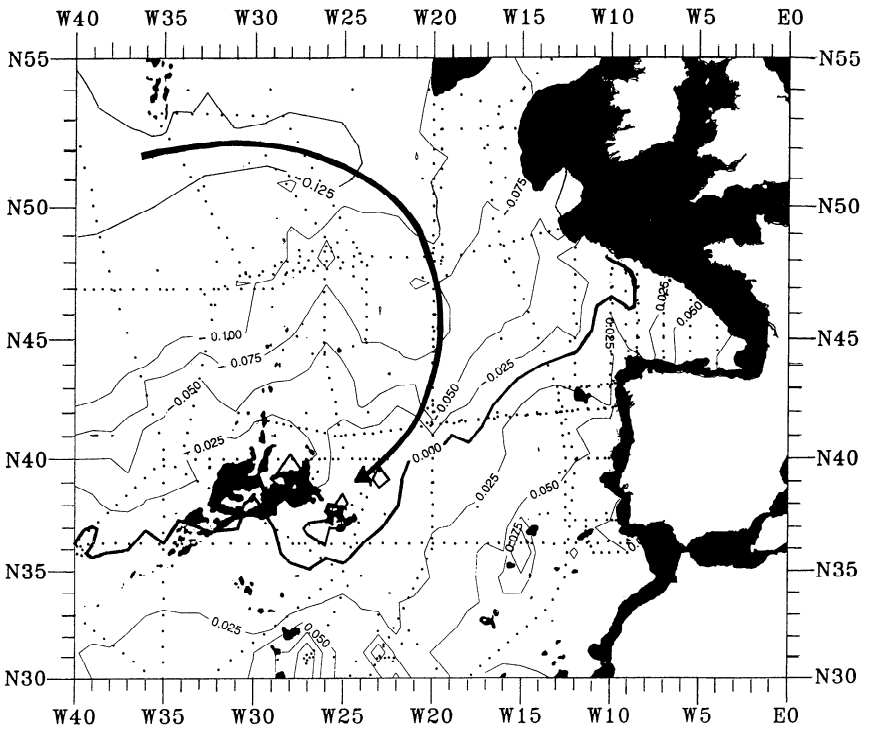

Figure 6. Minimum values of ΔS in the $32.25 < \sigma_{1,2} < 37.00$ density range and $P > 1000$ dbar for the complete data set. The arrow marks the main path of LSW circulation in the eastern basin, as suggested by the ΔS isopleths.

tongues or patches in Figure 6. The LSW-DMW front is itself slightly smoothed on this map when compared to individual sections.

3.3. Evidence for an Eastern Basin "Deep Western Boundary Current"

Figure 7a provides a detailed view of the Azores Plateau and neighboring hydrographic lines. Despite the large time span of these data (almost 8 years), a consistent view of a LSW vein flowing around the Azores Plateau can be inferred. Starting from the north, section 41N (Figure 5f) shows relatively pure ($\Delta S < -0.025$) LSW at 27°W–28°W, and section "40N" from the TOPOGULF data set (Figure 7b) shows a similar signal at 26°W–27°W. These features are most certainly signatures of a southward flow of relatively fresh LSW above the eastern flank of the MAR (Figure 7a). Farther south, similar cores of LSW present at 37°N–38°N on TPE (Figure 5c) and around 27°W on 36N (Figure 5g) mark the continuation of that vein as it flows round the 2000-m isobath at the eastern tip of the Azores Plateau. This topographically guided flow is still visible as a core of negative ΔS values on the TOPOGULF "South Azores" (SAZ) section (Figure 7c) but is no longer apparent farther downstream on 36N (Figure 5g). It is likely that the LSW flowing in the boundary current is transformed by mixing with surrounding water to finally lose its $\Delta S < 0$ characteristics in this region. Although the Oceanographer Fracture Zone (OFZ) at 35°N is located in the region of positive anomaly (Figure 6), the 35W section (Figure 5a) indicates that the water found closest to it in the eastern basin (at station 66) is much fresher at 2000 dbar than the water more to the south. This indicates an enhanced LSW influence at the entry of the fracture zone, most likely due to the continuation of the boundary current. The bathymetric peak at station 67 in Figure 5a marks the northern wall of the OFZ, and the water found north of that peak, notably the DMW present at station 68 (Figure 5a), belongs to the western basin. Considering the bathymetric configuration in the vicinity of the OFZ (Figure 7a), that water is likely to have crossed the MAR westward through either the OFZ or a deep passage just to the north of the fracture zone itself.

3.4. Evidence for a Northern Entry Into the Bay of Biscay

Figure 8 displays the vertical distribution of ΔS along two sets of meridional lines in the Bay of Biscay area, one gathered during cruise Phygas 42 in 1974 and the other during the Discovery cruises 181 and 189 in 1989 and 1990 (Table 1). Three of the 1974 sections, along 10°W, 8°30′W, and 7°W were repeated in 1989–1990, allowing direct comparisons. Although the 1974 CTD casts were limited to 2000 m depth, striking similitudes between the two data sets are revealed. The most notable agreement lies in the presence of the lowest ΔS values in the northern half of each section. LSW appears confined to the north of the Charcot Seamounts, which are the eastern extension of the Azores-Biscay Rise (Figure 1). In all sections of Figure 8 the LSW core is, however, not stuck to the continental slope, suggesting that a northwestward slope current carrying saltier water might exist inshore of it. Both series of sections show that the $\Delta S < 0$ signal does not reach the easternmost part of the Bay of Biscay, and one may wonder if the LSW recirculates westward within the patch of $\Delta S < 0$ or is transformed to $\Delta S > 0$ in the course of its eastward flow before subsequent westward recirculation south of the Charcot Seamounts.

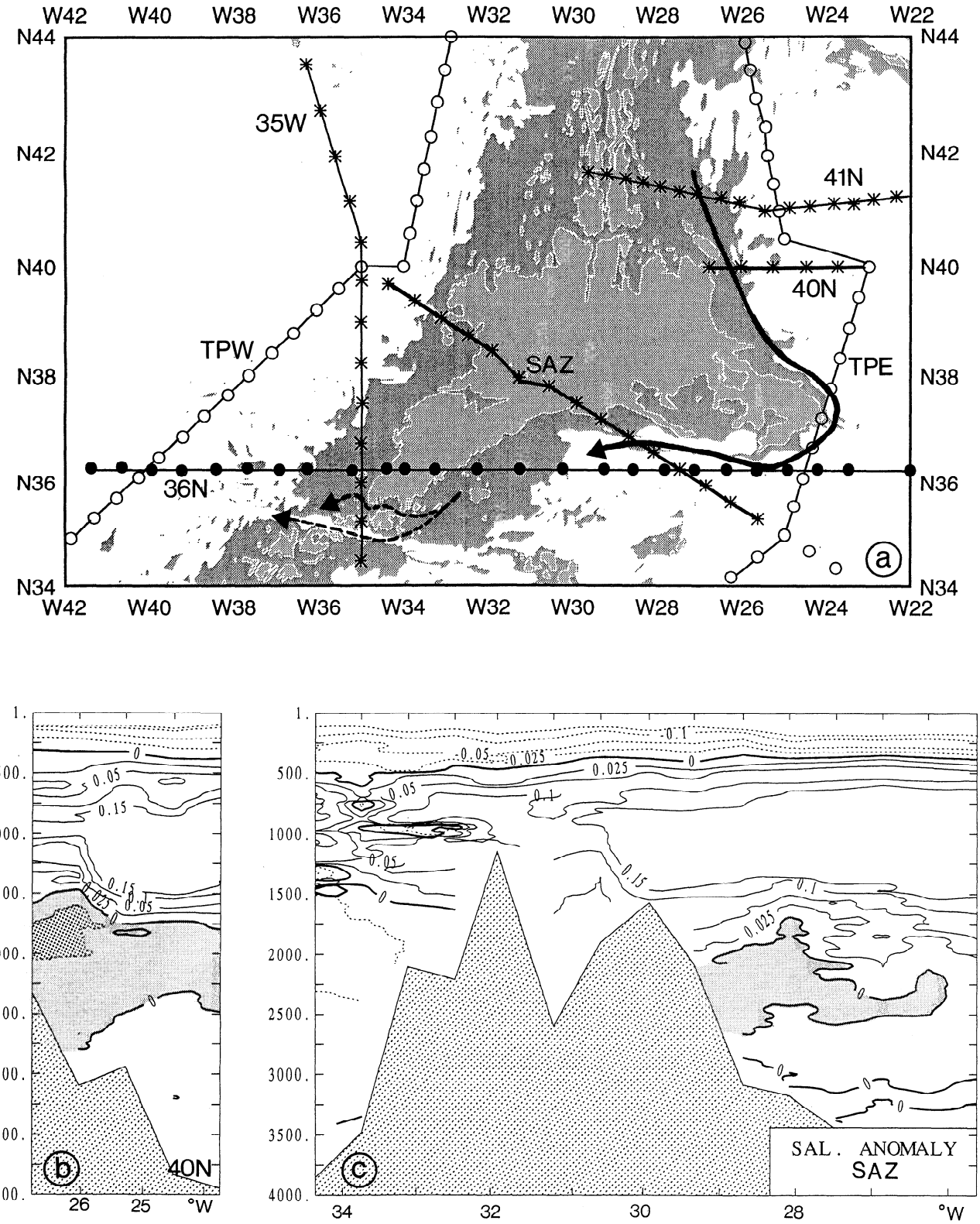

Figure 7. (a) Detailed view of the Azores Plateau data set (bathymetric contours 2000 and 3000 m), with a schematic representation of the LSW flow around the Azores Plateau (bold arrowed line). The dashed arrows mark the hypothesized LSW and DMW throughflows in and near the Oceanographer Fracture Zone. (b) and (c) Vertical distributions of ΔS along lines 40N and SAZ (bold segments on Figure 7a). LSW of $\Delta S < 0$ is shaded.

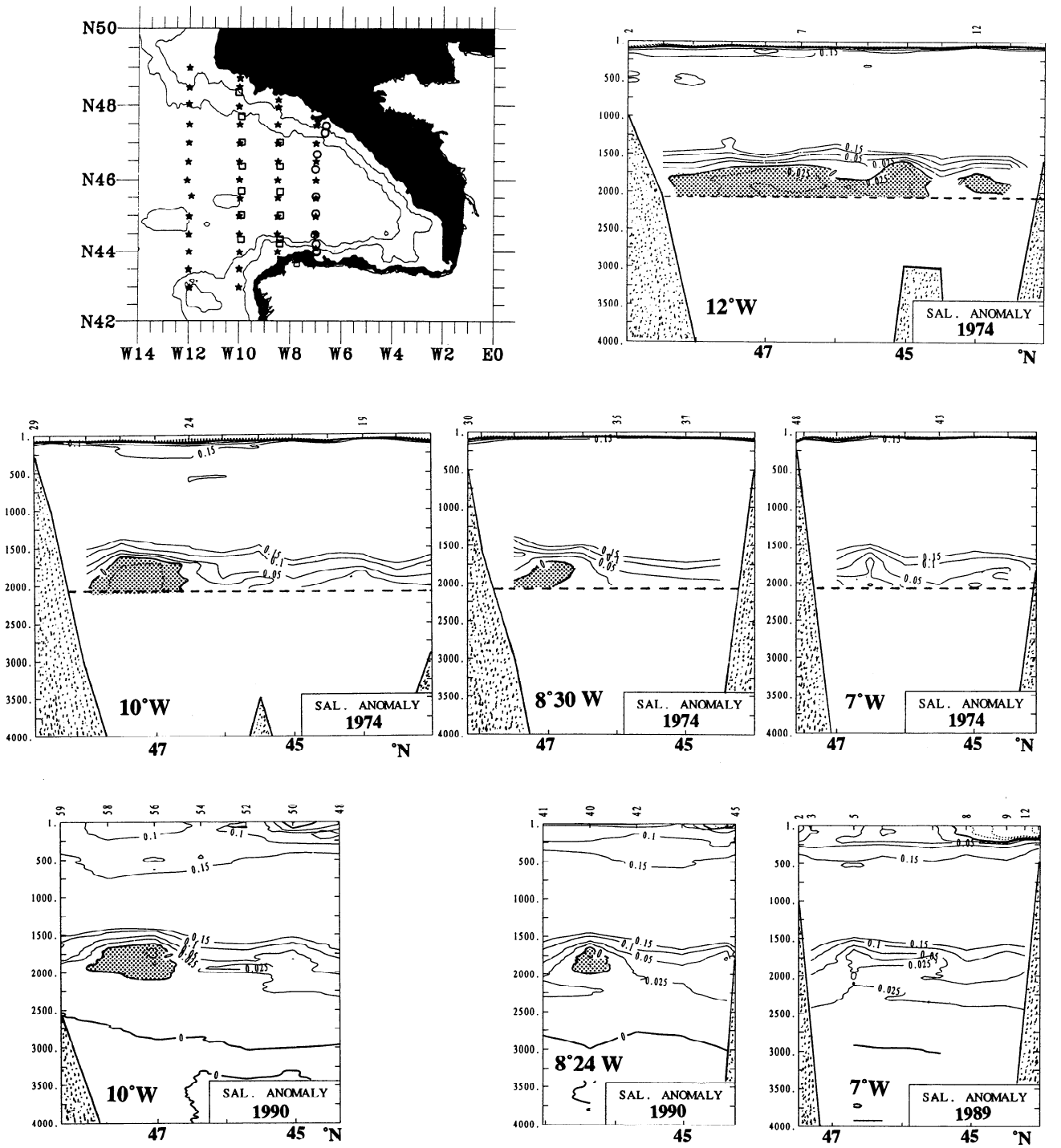

Figure 8. Vertical distributions of ΔS along meridional lines in the Bay of Biscay area. LSW of $\Delta S < 0$ is shaded.

4. Circulation and Transports at the LSW Level

The descriptive considerations in section 3 are now examined using the results of an inverse model of the eastern North Atlantic based on a data set close to that of Figure 1. A question arises as to whether transport calculations, inverse or direct, should be computed using the exactly measured hydrography or a smoothed one. Considering the nonsynopticity of the data set, the large mesoscale noise in the individual high-resolution sections, and the need for a method that constrains well the flow at middepth, we chose the *Mercier et al.* [1993] type of model which uses a smoothed hydrography and a large set of dynamical constraints. Therefore we expect to lose in the model results some details of the LSW pathways described above, but we aim at obtaining a large-scale circulation compatible with large-scale forcings, dynamics, and bathymetry. The inverse model was applied by *Paillet and Mercier* [1997] (hereafter referred to as PM97) to the eastern North Atlantic. Here we discuss the circulation and transports at the LSW level

associated with a slightly different solution, for which a few constraints have been modified. We depict only briefly the model formulation, details of which are given by Mercier et al. and Paillet and Mercier.

4.1. The Model

The PM97 model seeks a density field as close as possible to the hydrographic data and an absolute velocity field exactly nondivergent and in thermal wind balance, satisfying as well as possible dynamical constraints which are the planetary vorticity balance, the Ekman dynamics at the surface, mass, salt and heat conservations in a top-to-bottom integrated form, and specific transport constraints. The model is run on a regular grid of 1° latitude by 1.5° longitude horizontal resolution, between 24°N and 54°N and east of 35°W, with 58 levels on the vertical and a realistic bathymetry. The hydrographic data set is mostly composed of the deep CTD data of Table 1 gathered after 1980 (PHYGAS 42 and Discovery 81 or "41N" were not used, see PM97). An estimation of the density field is objectively mapped onto the regular grid from the original, irregular data set, as well as potential temperature and salinity fields. An horizontal smoothing on a scale of about 400 km results from that method. The horizontal and vertical velocity fields are obtained from the density field by vertical integrations of the thermal wind and continuity equations, respectively, with a condition of no flow across the bathymetry.

The problem unknowns are the density field, the velocity field at the reference level (taken as 2500 m or the bottom, if shallower), and a uniform lateral eddy mixing coefficient used in the tracer conservation constraints. Following *Tarantola and Valette* [1982], the inversion consists in minimizing the value of a scalar cost function, made of the sum of the weighted squared distances to the unknowns a priori values and of the weighted squared dynamical constraints residuals.

For this work, we improved PM97's set of transport constraints. They pointed out two weaknesses of their model solution that were likely to affect the LSW and DMW circulation:

4.1.1. Charlie-Gibbs Fracture Zone. PM97's solution lacks an outflow of ISOW toward the western basin in the CGFZ, which was measured using currentmeters as 2.4 ± 0.5 Sv (1 Sv = 10^6 m^3 s^{-1}) by *Saunders* [1994]. We imposed such an outflow and obtained a westward flow of 2.1 Sv across 35°W, between 52°N and 53°N and below 2000 m. Other estimates of that transport are higher [*Worthington and Volkmann*, 1965; *McCartney*, 1992; *Schmitz and McCartney*, 1993], but the smoothed hydrography and the dynamics of the model do not allow a higher transport to be forced without altering the realism of the solution (water being then simply "sucked in" from the western boundary at the next pair of grid points to the south).

4.1.2. Gulf of Cadiz. PM97 forced a 4 Sv MOW outflow across 8°W in the Gulf of Cadiz but noted a misrepresentation of that outflow in their solution, part of it turning directly southward to feed the Canary Current, whereas little MOW salt is actually found near the African coast. We therefore chose to constrain only a northern vein, imposing a westward flow of 4 Sv between 36°N and 37°N in the depth range [750–1500 m]. Half of it turns northward and northwestward, while the other half recirculates back eastward into the Gulf of Cadiz. The direct connection between the Gulf of Cadiz and the Canary Current at the MOW level no longer exists. The circulation at 1000 m (not shown) is nonetheless very similar to that of PM97 (their Figure 7d) except in the vicinity of the Gulf of Cadiz.

As in PM97, a solution that satisfies the set of constraints well within the allowed error bars is found. Such a solution is thought to be a good first-order estimate of the mean large-scale hydrography and circulation over the sampled period (1981–1993).

4.2. Model Circulation at the LSW Level

The model salinity and velocity fields at 1750 m are displayed in Figure 9. While displaying properties on an isopycnal could be more physically meaningful, the constant depth of 1750 m was chosen because it is a vertical level of the model grid and because the isopycnals are rather flat in that area around that depth, at least south of 50°N. The salinity field (Figure 9a) presents features and values similar to those shown by *Talley and McCartney* [1982] at the LSW potential vorticity minimum. The LSW-DMW front is horizontally smoothed and belongs to the 35.0–35.1 band. The 35.05 isohaline corresponds closely to the $\Delta S_{min} = 0$ of Figure 6 and is superimposed on the velocity field so as to materialize the southern boundary of LSW detectability.

The general trend of the circulation at 1750 m is an eastward crossing of the MAR north of 48°N, intensified around 30°W between 51°N and 53°N, followed by a weak and broad northward recirculation and a stronger southward recirculation in the middle of the eastern basin. To the west of the MAR, an eastward flow at 45°N–47°N recirculates southwestward without crossing the MAR. Although many features of that velocity field are consistent with those previously inferred from the ΔS field (Figures 4–8), others are not. Among the most notable agreements are the eastward flow above the MAR, its separation into two branches, and the marked southward flows in the middle of the basin and around the Azores Plateau. The southward branch west of the MAR was also suggested by the tracer distributions. One the other hand, a southern entry into the Bay of Biscay (Figure 9b) is present where a northern entry was suggested in section 3.4. This may be due to the difficulties of the inverse model in representing correctly small-scale currents.

Although the two-dimensional pictures of Figure 9 do not give the actual angle between the 3-D velocity vectors and 3-D isohalines, the tendency of water parcels to gain or lose salinity along the mean advective paths can be inferred from comparing Figures 9a and 9b. The conservation of salt being imposed in the model only as a top-to-bottom integrated budget, the flow is not locally constrained to parallel the isohalines. Over most of the domain the water is gaining salinity, which can be qualitatively accounted for by mixing (in a fluid of minimum salinity). *Bogden et al.* [1993, Figure 2.3] find cross-isohaline flows of the same order of magnitude (and similar circulation patterns at 2000 m), although their inverse model is constrained to minimize density mixing locally. The circulation near the LSW-DMW front is generally southwestward along the 35.05 isohaline, but significant southward cross-frontal flows exist at 15°W–20°W and south of the Azores Plateau. The details of these flows may not be realistic, as the data used to build the gridded hydrographic fields are nonsynoptic and perturbated by mesoscale features. Nevertheless, the southward flowing LSW cannot leave the eastern basin without ultimately crossing the $S = 35.05$ isohaline. Furthermore, an important feature of the model circulation at 1750 m is that there is no arrival of water from south of 30°N. This means that the whole

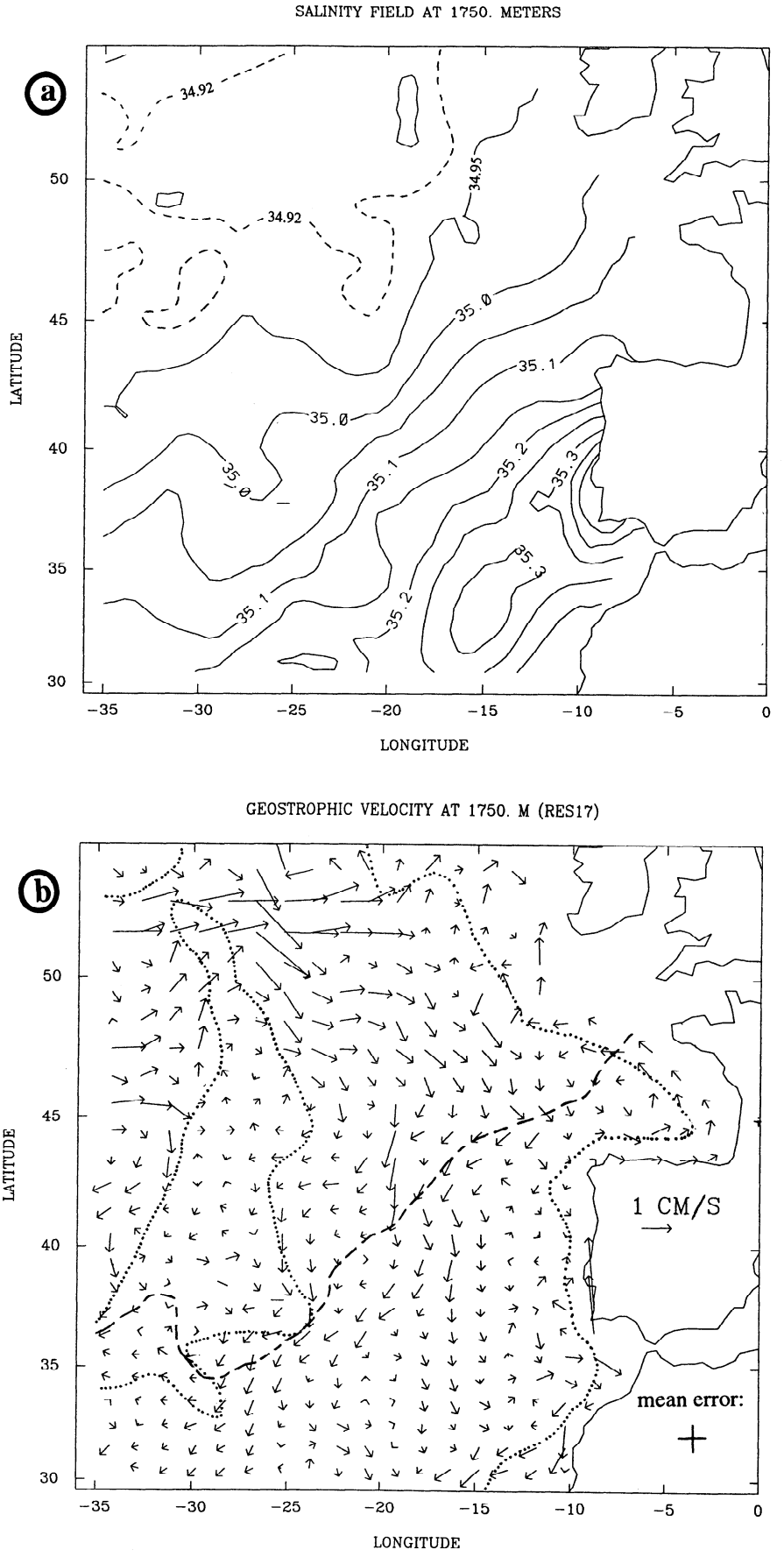

Figure 9. (a) Salinity field at 1750 m, as gridded for the inverse model. (b) Inverse model velocity field at 1750 m. The solid line is the $S = 35.05$ isocontour of Figure 9a. Dotted lines represent the model 3000 m isobath.

region is fed, at 1750 m, by water from the Labrador Sea, what was named DMW being simply LSW that has been transformed by mixing with the MOW above. The LSW-DMW front, which does not appear as a zone of water mass convergence, must then result from the transformation of the relatively fresh LSW into saltier DMW by a rapid mixing process. Double diffusion, which can efficiently transport salt downward from the overlying MOW, is a very likely candidate. We show in the appendix that double diffusion in the region may account for a horizontal salinity gradient of order 0.1 in 200 km. This value is indeed representative of the LSW-DMW transition, from $S = 35.0$ to $S = 35.1$, observed on a large scale by *Talley and McCartney* [1982], *Cunningham and Haine* [1995a], or in Figure 9a. As discussed in sections 5 and 6, physical processes like baroclinic instability may lead locally to a further sharpening of the LSW-DMW front. Double diffusion is certainly also active away from the area of the front, as observations of thermohaline staircases at many locations below the main MOW tongue [*Tsuchiya et al.*, 1992] suggest, which is consistent with the mean flow in Figure 9a heading toward higher salinity over most of the domain.

A recent planetary geostrophic model (M. A. Spall, A simple model of the large scale circulation of Mediterranean Water and Labrador Sea Water, submitted to *Deep Sea Research*, 1997, hereinafter referred to as Spall, submitted manuscript, 1997) suggests that double diffusion between MOW and LSW might not only have a "passive" transformation effect but might also play an important dynamical role and contribute to drive both water masses circulation. In Spall's model, the downward diapycnal velocities that are required to balance double diffusion drive the LSW eastward to the eastern basin at about 50°N, then southward, before the water resulting from the mixing is expelled to the western basin at subtropical latitudes.

A remaining question is that of the reliability of the inverse model circulation. The postinversion amplitude of the errors on the velocity components is around 0.5 cm/s (against 1.1 cm/s before inversion), that is, of the same order as the velocities themselves (Figure 9b). One must therefore admit that the circulation of Figure 9b is highly uncertain. Nevertheless, it is quite consistent with what ourselves and previous authors [*Talley and McCartney*, 1982; *Harvey and Arhan*, 1988; *Cunningham and Haine*, 1995a] deduced from the tracer fields. It has also been a robust feature of the model solution during its development, whatever the choice of the boundary conditions, weights or reference level were made. We note, finally, that such a well-behaved circulation is obtained near the a priori reference level of 2500 m, where an insufficiently constrained method would lead to a near-zero field.

4.3. LSW Transports

The usual choice of a middepth reference level for geostrophic calculations may explain why only few estimates of the LSW transports in the eastern North Atlantic are available in the literature. *McCartney* [1992] provides a review and analysis of most of these estimates, further compiled by *Schmitz and McCartney* [1993, Figure 11] to infer quantitative transports in the 3°–4°C layer: fed by a part of the 7 Sv formation rate in the Labrador Sea and by a Subpolar Gyre recirculating component, a total eastward flow of 13 Sv is seen crossing the MAR in the vicinity of the CGFZ and further recirculates northward. The southward recirculation in the eastern basin, although schematized by *McCartney* [1992, Figure 8], is not quantitatively estimated. *Gana and Provost* [1993] provide the numbers of 1 ± 0.7 Sv of LSW flowing southward along each side of the MAR, but their inverse model is restricted to the vicinity of the MAR.

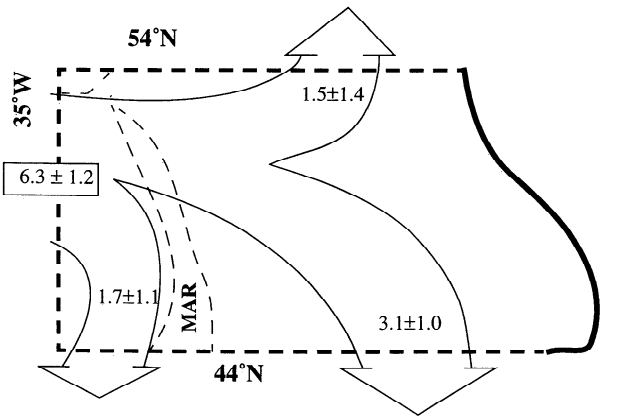

Figure 10. Scheme of the inverse model LSW transport. Numbers are in Sv (10^6 m^3 s^{-1})

In our inverse model, the total eastward transport across 35°W in the 3°–4°C layer, between 44°N and 54°N, amounts to 10 ± 2 Sv, a figure comparable to the 13 Sv of *Schmitz and McCartney*'s [1993] scheme. However, a part of the 3°–4°C layer water cannot be considered as LSW, being either too shallow (and stratified) or too saline. Considering only the water inside the broad property range defined by *Wright and Worthington* [1970] to characterize LSW, that is $3°C < \theta < 4°C$ and $S < 34.94$, and adding the criterion $P > 1000$ dbar, the model eastward transport between 44°N and 54°N reduces to 6.3 ± 1.2 Sv. Figure 10 summarizes how that inflow recirculates across the 44°N and 54°N parallels. In order to balance the inflow by the same amount of outflows, the core characteristics of the LSW had to be widened to take into account the mixing with surrounding water that occurs during the recirculation. The characteristics of the LSW recirculating northward across 54°N were extended to $S < 35.0$, while keeping $3°C < \theta < 4°C$, to find a transport of 1.5 ± 1.4 Sv. Those of the LSW that recirculate southward across 44°N were extended to $2.8°C < \theta < 4°C$ and $S < 35.0$, which yields transports of 1.7 ± 1.1 Sv west of the MAR and 3.1 ± 1.0 Sv east of the MAR. To be compatible with the planetary vorticity balance, the southward flow of LSW in the 30°N–50°N band requires some compression of the fluid columns, which is mostly achieved in the inverse model by a downwelling from above, amounting to 2.3 Sv across the 1500 m depth surface. This feature is also consistent with Spall's (submitted manuscript, 1997) analytic model.

To summarize, of the 6.3 Sv of LSW crossing 35°W westward, about one fourth recirculates southward in the western basin, another fourth recirculates northward, and the remaining half recirculates southward in the eastern basin. The northward recirculation seems weak when compared to *Schmitz and McCartney*'s [1993] value (13 Sv) yet is consistent with the potential vorticity distribution in *Talley and McCartney*'s [1982] map showing rather diluted northeastern extensions in the Rockall Trough and the Iceland Basin. Of the 1.5 Sv of LSW which turns northward in our solution, about 1.2 Sv heads toward the Iceland Basin, west of 20°W, while the remaining 0.3 Sv feed the Rockall Trough east of 20°W.

We have considered so far the mean circulation and water mass distributions, but it is clear from Figures 4 and 5 that mesoscale perturbations exist at the LSW level. We now focus on some of these mesoscale structures and their possible origin.

5. Mesoscale Structures in the Vicinity of the LSW/DMW Front

Colin de Verdière et al. [1989] and *Schauer* [1989], analyzing current meter and hydrographic data, respectively, showed the existence at about 48°N of cyclonic concave lenses depleted of LSW, with a velocity structure intensified between 1500 and 2500 m depth. These structures were thought to originate from instabilities of middepth jets or thermohaline fronts like the LSW-ISOW transition in the Charlie Gibbs Fracture Zone or the LSW-DMW front in the eastern basin. An anticyclonic lens full of LSW, found in the western North Atlantic during the Local Dynamics Experiment, was proposed to have formed in the vicinity of the Grand Banks of Newfoundland, through instability of the Deep Western Boundary Current by *Elliott and Sanford* [1986] or through winter convection in the Labrador Sea by *McWilliams* [1985].

Our data set provides other examples of such mesoscale, subthermocline lenses. Figures 4 and 5 reveal numerous small-scale perturbations above 2500 dbar. First, trying to detect high-salinity lenses in the domain of dominant LSW influence, we find that all the middepth high-salinity structures have their ΔS maximum around 1000 dbar, but some of them have a deep reaching influence with positive ΔS values down to more than 1500 dbar: the most notable of these are found at station 31 of TPW (40°N, Figure 5b), station 53 of TPE (43°N, Figure 5c), stations 45 and 48 of 20W (43°N and 41.5°N, Figure 5d), and stations 6 and 15 of 41N (27.5°W and 23°W, Figure 5f). All these structures are found in the vicinity of the LSW-DMW front.

Inside the DMW domain, several small lenses with negative ΔS in the 1500–2500 dbar range stand out, marked by arrows on Figure 5: at station 18 of TPW (35°N, Figure 5b), at station 31 of TPE (35.5°N, Figure 5c), at station 20 of 41N (20°W, Figure 5f), and at stations 51 and 69 of 36N (39°W and 24.5°W). These "LSW eddies" are also found in the vicinity of the LSW-DMW front.

Another example of a LSW eddy is provided in Figure 11. It displays the 6-month trajectory of a RAFOS float launched at 34°15′N, 25°20′W at about 2000 dbar during the SEMAPHORE 93 experiment [*Tychensky et al.*, 1998]. The float began to rotate anticyclonically with a 5–6 day period, while propagating to the northeast at about 0.8 cm/s, then after 2 months it headed toward the southwest at a mean velocity of 1.5 cm/s. At the end of its 6-month mission, its rotation period had increased to about 9 days. The translation effects being filtered out, the apparent radius of the eddy remained between 10 and 14 km, and the azimuthal velocities remained between 5 and 12 cm/s, yielding Rossby numbers of order 0.12. Such properties fall within the range defined by *McWilliams* [1985] to characterize "submesoscale coherent vortices." The net southwestward displacement is consistent with its anticyclonic nature. Of the 10 RAFOS floats launched at the same level in a 500 km × 500 km area during the SEMAPHORE 93 experiment, only this one presented such a rotating trajectory. CTD casts down to 2500 dbar were carried out during the same cruise. The insert in Figure 11, which displays the θ/S diagrams obtained at the launching point of the RAFOS float and at the four nearest CTD stations, shows that the float was launched in a relatively fresh water with slightly negative ΔS values between 1900 and 2200 dbar. It is thus a "LSW eddy" that was sampled, most likely similar to the lenses of negative ΔS observed above. All these eddies have a diameter smaller than 80 km, which would allow to classify them as "submesoscale" eddies, and their homogeneous core suggests that they may all be anticyclones.

To summarize, we have located six LSW lenses, most probably anticyclonic, south of the LSW-DMW front, and six mesoscale DMW intrusions north of the front that are likely to be cyclonic, because of the relatively high PV associated with the DMW and their resemblance to *Schauer*'s [1989] salty concave lens found further north. This strongly suggests that the flow in the vicinity of the front, which the inverse model suggests to be dominantly southwestward along it, is unstable an sheds eddies containing water with ΔS values opposite to their environments.

Spall [1994] showed that the mean flow in the basin, vertically sheared between the MOW and LSW-DMW, always satisfies a generalized (for nonzonal flows) necessary condition for baroclinic instability. In his model, instability develops with maximum energy at the MOW level, where it forms large zonal meanders which further split into subthermocline eddies of less than 100 km scale. To know more specifically if the flow in the vicinity of the LSW-DMW front was likely to be unstable, we checked the classical necessary condition for baroclinic instability [*Charney and Stern*, 1962], which states that the meridional potential vorticity gradient $\partial q/\partial y$ changes sign along the vertical in an unstable zonal current. Figure 12 displays the distribution of q with latitude at 1500 and 2500 dbar along the 20W line that presents a marked LSW-DMW transition at 41°N. There, $\partial q/\partial y$ is positive at 2500 dbar and negative at 1500 dbar with in both cases relatively large values of that gradient. Thus the necessary condition for baroclinic instability is met. If that instability occurs, a middepth intensified flow involving mostly baroclinic modes higher than 2, perturbations should develop on scales of the order of the second radius of deformation, which would account for the smallness of the produced vortices.

6. Discussion

This study proposed a new characterization of the LSW by a "salinity anomaly" ΔS relative to a standard θ-S curve, the main advantage of which being to show where the influence of each of the intermediate water masses dominates. It allows an easy detection of the LSW-DMW front and of small-scale anomalies on each side of that front. Although the data used here were collected over a long period, a remarkable consistency in the ΔS distributions along the different hydrographic lines was found, confirming that the variations of the LSW properties at its source are largely attenuated before entering the eastern North Atlantic. It also suggests that the main features of the LSW circulation remained nearly constant during the sampled period (they are even comparable to those described by *Talley and McCartney* [1982] from their earlier data set). This justifies the inverse computation of the LSW circulation from our data. The model using a smoothed hydrography, some of the details provided by the individual high-resolution sections are lost, but we obtain a circulation consistent with the large-scale features shown by the data.

The southward transport of LSW is of interest because it

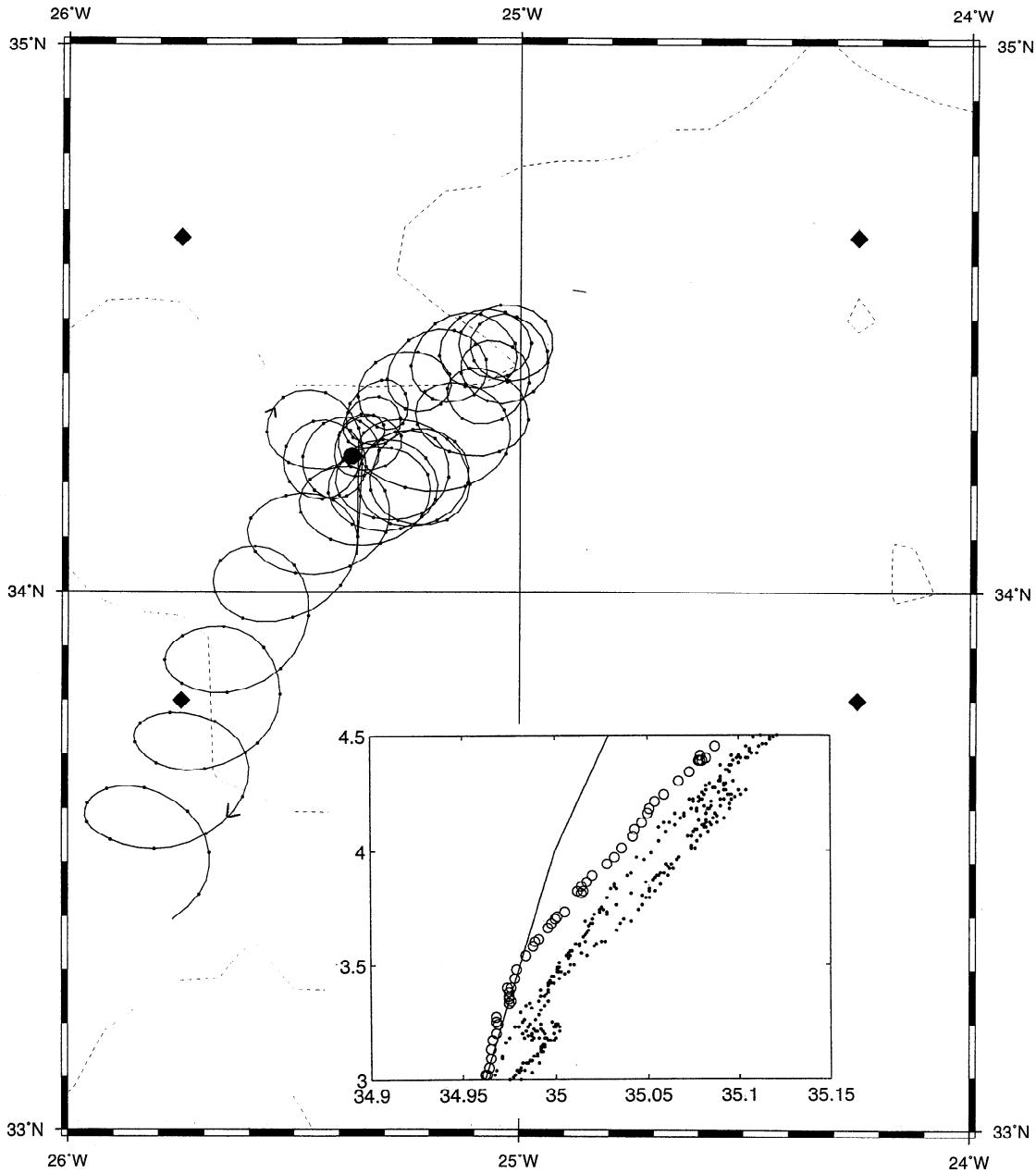

Figure 11. Six-month trajectory of a RAFOS float launched at 2000 dbar southeast of the Azores. Insert shows θ/S plots at the RAFOS launching point (circles) and at the four closest CTD stations of the same cruise (dots). The locations of these stations are shown with a circle and four diamonds, respectively, on the main figure.

participates in the intergyre exchanges and the global oceanic overturning. The inverse model suggests that 4.8 ± 1.4 Sv of LSW recirculate southward across 44°N east of 35°W, of which 3.1 ± 1.0 Sv flow in the eastern basin. These numbers should be added to the net LSW transport by the Deep Western Boundary Current (about 4 Sv according to *Schmitz and McCartney* [1993]) to get the actual contribution of LSW to the meridional overturning cell.

The LSW-DMW front does not result from the convergence of the two different water masses but might be created by double diffusive mixing of the southward flowing LSW with the overlying MOW. This again points to the contribution of the LSW to the North Atlantic Deep Water complex which constitutes the cold segment of the global thermohaline cell: LSW is generally recognized [*Wüst*, 1935] as providing the "middle" variety of this water mass in the DWBC, detected at equatorial latitudes at about 2200 m depth and associated with high oxygen values. Shallower in the water column, the high salinity of the "upper" NADW, on the other hand, can be traced back to the saltier water of the eastern basin subtropical latitudes, here named DMW. This study shows that DMW itself is partly composed of LSW so that an influence of the latter water mass is also brought to the upper NADW via the eastern basin. A recent reproduction of the transit of LSW in the eastern basin in a planetary geostrophic model (Spall, submitted manuscript, 1997) leads to a similar view.

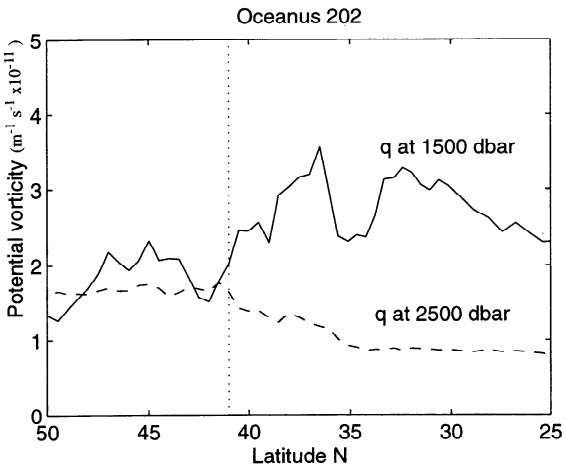

Figure 12. Evolution with latitude of the large-scale potential vorticity q at 1500 and 2500 dbar along the 20W section. The dotted vertical line marks the latitude of the LSW-DMW front.

An outstanding circulation feature deduced from the hydrography is a vein of LSW that flows clockwise along the slope of the Azores Plateau, an eastern basin counterpart of the Deep Western Boundary Current found along the American continental slope. As the LSW seen in the eastern basin is mostly confined to the northwest of the Azores-Biscay Rise, its southward recirculation is apparently deflected (to the right) by that ridge. That topographic steering might be the cause of the southwestward flow observed between 40°N and 45°N in the inverse model field (Figure 9b). That flow, being unable to cross the Azores Plateau, may give rise to a boundary-intensified vein.

Several subthermocline eddies were described in section 5. Former studies pointed out the existence of mesoscale cyclonic structures containing DMW north of the LSW-DMW front. The present data set shows that anticyclonic counterparts containing LSW exist south of the front, most likely generated by baroclinic instability. That process was probably active when the "20W" transect crossed the front: This line shows a succession of anomalies of both signs (Figure 5d) near 41°N, suggesting that the front was meandering. The salinity transition at the front is much more abrupt (0.1 in 50 km) than in other sections, possibly a result of a local frontogenesis that can be triggered by baroclinic instability. We also showed that a necessary condition for baroclinic instability was met by the potential vorticity distribution there (Figure 12). Instability of the mean meridional flow at the MOW level as discussed by *Spall* [1994] is also likely to be active at the LSW-DMW level and to participate in the cross-isohaline eddy transport there. The southward translation of submesoscale, coherent vortices containing LSW might play a nonnegligible role in the transport of that watermass across the LSW-DMW front, a process that the inverse model may wrongly interpret as being due to steady advection. At this stage, however, attempts to quantify this process remain hazardous.

Appendix: Could Double Diffusion Alone Build the LSW-DMW Front?

The double-diffusion (or salt-fingering) process is known to be active only when the density ratio

$$R_\rho = \left(\alpha \frac{\partial T}{\partial z}\right) \Big/ \left(\beta \frac{\partial S}{\partial z}\right)$$

(where α and β are the thermal expansion and haline contraction coefficients) becomes lower than some critical value (typically $R_\rho \approx 1.7$ [*Schmitt*, 1981]). *Daniault et al.* [1994] pointed out that if MOW with western Gulf of Cadiz characteristics and LSW with CGFZ characteristics could be brought to meet and superpose, the resulting density ratio at their boundary would be $R_\rho = 1.2$, well inside the domain favorable for double diffusion. This naturally does not occur in the real ocean without preliminary modifications of both water masses, yet *Tsuchiya et al.* [1992] observed low density ratios ($R_\rho < 1.5$) between 30°N and 45°N and well-defined thermohaline staircases indicative of active double diffusion between 29°30′N and 39°N along the 20W section. In order to check if double diffusion could build up the LSW-DMW front, we assume that the process is triggered near the northern side of the front, and consider the simplest balance between horizontal advection and vertical, Fickian-like double diffusion:

$$\mathbf{u} \cdot \nabla S = K_{\mathrm{vDD}} \frac{\partial^2 S}{\partial z^2}$$

where K_{vDD} is the vertical diffusion coefficient associated with double diffusion, compared to which the coefficients associated with other mixing processes are assumed negligible.

Taking $\partial^2 S/\partial z^2 = 10^{-6}$ m^{-2} from the large-scale hydrography, $K_{\mathrm{vDD}} = 5 \times 10^{-4}$ m^2 s^{-1} (half the typical maximum oceanic value given by *Schmitt* [1981]), and a velocity component normal to the isohalines of $u_\perp = 10^{-3}$ m s^{-1} from the basin-averaged inverse model results, we obtain a typical value of the salinity gradient of 5×10^{-7} m^{-1}, or 0.1 in 200 km.

Acknowledgments. We would like to thank Herle Mercier for his thorough help with the inverse modeling and Aude Tychensky and Ruth Curry for providing us with the Rafos data and the central Labrador Sea hydrographic properties, respectively. Thanks are also due to Xavier Carton, Cecilie Mauritzen, and Mike Spall for useful comments on the manuscript. The help of Catherine Fontaine, Philippe Le Bot, and Pierre Doaré for preparing the figures is gratefully acknowledged. M. A. was supported by IFREMER grant 210160 and by contract 25-95 from EPSHOM (Etablissement Principal du Service Hydrographique et Océanographique de la Marine). M. S. M. was supported by the U.S. National Science Foundation grant OCE95-29606 and the National Ocean and Atmosphere Administration Atlantic Climate Change Program grant NA36GP0137. This is Woods Hole Oceanographic Institution contribution 9481.

References

Arhan, M., A. Billant, A. Colin de Verdière, L. Mémery, and P. Treguer, CTD-02 and nutrients along the eastern boundary of the North Atlantic Ocean from 60°N to 20°N, *Bord-Est Data Rep. 13*, vol. 1, 115 pp., Campagnes Océanogr. Fr., Publ. IFREMER, Brest, France, 1991a.

Arhan, M., A. Billant, A. Colin de Verdière, N. Daniault, and R. Prego, Hydrography and velocity measurements offshore from the Iberian Peninsula. *Bord-Est Data Rep. 15*, vol. 2, 232 pp., Campagnes Océanogr. Fr., Publ. IFREMER, Brest, France, 1991b.

Arhan, M., A. Colin de Verdière, and L. Mémery, The eastern boundary of the subtropical North Atlantic, *J. Phys. Oceanogr., 24*, 1295–1316, 1994.

Armi, L., and N. A. Bray, A standard analytic curve of potential temperature versus salinity for the western North Atlantic, *J. Phys. Oceanogr., 12*, 384–387, 1982.

Bogden, P. S., R. E. Davis, and R. Salmon, The North Atlantic circulation: Combining simplified dynamics with hydrographic data, *J. Mar. Res., 51*, 1–52, 1993.

Charney, J. G., and M. E. Stern, On the stability of internal baroclinic jets in a rotating atmosphere, *J. Atmos. Sci.*, *19*, 159–172, 1962.

Colin de Verdière A., H. Mercier, and M. Arhan, Mesoscale variability transition from the western to the eastern Atlantic along 48°N, *J. Phys. Oceanogr.*, *19*, 1149–1170, 1989.

Cunningham, S. A., and T. W. N. Haine, Labrador Sea water in the eastern North Atlantic, I, A synoptic circulation inferred from a minimum in potential vorticity, *J. Phys. Oceanogr.*, *25*, 649–665, 1995a.

Cunningham, S. A., and T. W. N. Haine, Labrador Sea water in the eastern North Atlantic, II, Mixing dynamics and the advective-diffusive balance, *J. Phys. Oceanogr.*, *25*, 666–678, 1995b.

Curry, R. G., M. S. McCartney, and T. M. Joyce, Oceanic transport of subpolar climate signals to mid-depth subtropical waters, *Nature*, *391*, 575–577, 1997.

Daniault, N., J. P. Mazé, and M. Arhan, Circulation and mixing of Mediterranean water west of the Iberian Peninsula, *Deep Sea Res.*, *41*(11–12), 1685–1714, 1994.

Elliott, B. A., and T. B. Sandford, The subthermocline lens D1, I, Description of water properties and velocity profiles, *J. Phys. Oceanogr.*, *16*, 532–548, 1986.

Fruchaud-Laparra, J. Le Floch, C. Le Roy, J. Y. Le Tareau, and F. Madelain, Etude hydrologique des variations saisonnières dans le proche Atlantique en 1974, *Rapp. Sci. Tech.*, *30*, 108 pp., Cent. Natl. pour l'Explor. des Océans, Brest, France, 1976.

Gana, S., and C. Provost, Circulation and fluxes of the central North Atlantic in 1983/1984 estimated by inverse analysis of 'Topogulf' hydrographic data, *J. Mar. Syst.*, *4*, 67–92, 1993.

Griffiths, G. S., et al., CTD oxygen, trace, and nutrients data from RRS *Charles Darwin* cruises 58/59 in the NE Atlantic as part of Vivaldi '91, *Rep. 296*, 51 pp., Inst. of Oceanogr. Sci., Deacon Lab., Wormley, England, 1992.

Harvey, J., and M. Arhan, The water masses of the central North Atlantic in 1983–84, *J. Phys. Oceanogr.*, *12*, 1856–1875, 1988.

Hendry, R. M., Hydrographic measurements from C. S. S. *Hudson* cruise 82-002, *Can. Tech. Rep. Hydrog. Ocean Sci.*, *118*, 112 pp., Bedford Inst. of Oceanogr., Dartmouth, Nova Scotia, 1989.

King, B. A., S. G. Alderson, S. Bacon, T. J. P. Gwilliam, C. Hirst, R. Paylor, J. F. Read, and J. C. Swallow, CTDO station data from the north east Atlantic from RRS *Discovery* cruise 189, *Rep. 287*, Inst. of Oceanogr. Sci., Deacon Lab., Wormley, England, 1991.

Lazier, J. R. N., Oceanographic conditions at Ocean Weather Ship *Bravo*, 1964–1974, *Atmos. Ocean*, *18*(3), 227–238, 1981.

Levitus, S., *Climatological Atlas of the World Ocean*, *NOAA Prof. Pap.*, *13*, 173 pp., Natl. Oceanic and Atmos. Admin., Silver Spring, Md., 1982.

McCartney, M. S., Recirculating components to the deep boundary currents of the northern North Atlantic, *Prog. Oceangr.*, *29*, 283–383, 1992.

McWilliams, J. C., Submesoscale, coherent vortices in the ocean, *Rev. Geophys.*, *23*, 165–182, 1985.

Mercier, H., M. Ollitrault, and P. Y. Le Traon, An inverse model of the North Atlantic general circulation using Lagrangian float data, *J. Phys. Oceanogr.*, *23*, 689–715, 1993.

Paillet, J., and H. Mercier, An inverse model of the eastern North Atlantic general circulation and thermocline ventilation, *Deep Sea Res., Part I*, *44*, 1293–1328, 1997.

Pingree, R. D., A component of Labrador sea water in the Bay of Biscay, *Limnol. Oceanogr.*, *18*, 711–718, 1973.

Read, J. F., R. T. Pollard, and C. Hirst, CTD data from the north east Atlantic, April 1989, collected on RRS *Discovery* cruise 181, *Rep. 285*, 157 pp., Inst. of Oceanogr. Sci., Deacon Lab., Wormley, England, 1991.

Roemmich, D., and C. Wunsch, Two transatlantic sections: Meridional circulation and heat flux in the subtropical sub-Atlantic Ocean, *Deep Sea Res.*, *32*, 619–664, 1985.

Saunders, P. M., Circulation in the eastern North Atlantic, *J. Mar. Res.*, *40*, suppl., 641–657, 1982.

Saunders, P. M., The accuracy of measurements of salinity, oxygen and temperature in the deep ocean, *Phys. Oceanogr.*, *16*, 189–195, 1986.

Saunders, P. M., The flux of overflow water through the Charlie-Gibbs Fracture Zone, *J. Geophys. Res.*, *99*, 12343–12355, 1994.

Schauer, U., A deep saline cyclonic eddy in the West European Basin, *Deep Sea Res.*, *36*, 1549–1565, 1989.

Schmitt, R. W., Form of the temperature-salinity relationship in the central water: Evidence for double diffusive mixing, *J. Phys. Oceanogr.*, *11*, 1015–1026, 1981.

Schmitz, W. J., and M. S. McCartney, On the North Atlantic circulation, *Rev. Geophys.*, *31*, 29–49, 1993.

Scripps Institution of Oceanography (SIO), Transient tracers in the ocean—North Atlantic study, 1 April–19 October 1981, shipboard physical and chemical data report, Univ. of Calif., San Diego, March 1986.

Spall, M. A., Mechanism for low-frequency variability and salt flux in the Mediterranean salt tongue, *J. Geophys. Res.*, *99*, 10121–10129, 1994.

Talley, L. D., and M. S. McCartney, Distribution and circulation of Labrador sea water, *J. Phys. Oceanogr.*, *12*, 1189–1205, 1982.

Tarantola, M., and B. Valette, Generalized nonlinear problems solved using the least squares criterion, *Rev. Geophys.*, *20*, 219–232, 1982.

TOPOGULF Group, The TOPOGULF data report vol. 1: CTD, O_2 and nutrients, *Ber. 154*, 183 pp., Inst. für Meereskunde, Kiel, Germany, 1986.

Tsuchiya, M., L. D. Talley, and M. S. McCartney, An eastern Atlantic section from Iceland southward across the equator, *Deep Sea Res.*, *39*, 1885–1917, 1992.

Tychensky, A., P.-Y. Le Traon, F. Hernandez, and D. Jourdan, Large structures and temporal change in the Azores Front during the SEMAPHORE experiment, *J. Geophys. Res.*, in press, 1998.

Worthington, L. V., and G. H. Volkmann, The volume transport of the Norwegian Sea overflow water in the North Atlantic, *Deep Sea Res.*, *12*, 667–676, 1965.

Wright, W. R., and L. V. Worthington, The water masses of the North Atlantic Ocean—A volumetric census of temperature and salinity, in *Serial Atlas of the Marine Environment*, folio 19, 8 pp., 7 plates, Am. Geogr. Soc., New York, 1970.

Wüst, G., Schichtung und Zirkulation des Atlantischen Ozeans: Die Stratosphäre, *Wiss. Ergebn. Dtsch. Atlant. Exped. 'Meteor' 6*, *1*(2), 109–288, 1935 (English translation, *The Stratosphere of the Atlantic Ocean*, edited by W. J. Emery, 112 pp., Amerind, New Delhi, 1978.)

M. Arhan, Laboratoire de Physique des Oceans (Unité Mixte CNRS-IFREMER-Université), IFREMER, Centre de Brest, B.P. 70, 29280 Plouzané, France.

M. S. McCartney, Woods Hole Oceanographic Institution, Woods Hole, Massachusetts, 02543.

J. Paillet, Service Hydrographique et Oceanographique de la Marine (Centre Militaire d' Océanographie), 13, rue du Chatellier, B. P. 426, 29275 Brest Cedex, France. (e-mail: paillet@shom.fr)

(Received March 26, 1997; revised October 9, 1997;
accepted December 1, 1997.)